AIAA 98-0298

Mars Pathfinder Rarefied Aerodynamics: Computations and Measurements

James N. Moss
Robert C. Blanchard
Richard G. Wilmoth
Robert D. Braun
NASA Langley Research Center
Hampton, VA 23681-0001

36th AIAA Aerospace Science Meeting & Exhibit
January 12-15, 1998/Reno, NV

MARS PATHFINDER RAREFIED AERODYNAMICS: COMPUTATIONS AND MEASUREMENTS

James N. Moss*, Robert C. Blanchard†, Richard G. Wilmoth‡, and Robert D. Braun§
NASA Langley Research Center
Hampton, Virginia

ABSTRACT

On July 4, 1997, after traveling close to 500 million km, the Pathfinder spacecraft successfully completed entry, descent, and landing at Mars. In the present paper, the focus is on the hypersonic rarefied portion of Pathfinder's atmospheric entry where the synergy of flight measurements, aerodynamic calculations, and atmospheric modeling tools are used to extract Pathfinder's attitude and the freestream density. Accuracy of the capsule aerodynamics directly impacts the inferred atmospheric properties extracted from deceleration measurements made by on-board accelerometers. The range of rarefaction considered in this study extends from the free molecular to continuum conditions and angles of attack from 0 to 30 deg. The aerodynamic computations are made with free-molecular and direct simulation Monte Carlo codes. The calculations show that Pathfinder is statically unstable for much of the transitional rarefied regime. Due to the relatively modest forces and the gyroscopic motion of the spacecraft, the angle of attack excursions were less than 5 deg as inferred from force measurements for the rarefied portion of entry and approached a nominal zero degree trim angle near hypersonic continuum conditions.

*Aerospace Engineer, Aerothermodynamics Branch, Aero- and Gas-Dynamics Division, Fellow AIAA.
†Aerospace Engineer, Aerothermodynamics Branch, Aero- and Gas-Dynamics Division, Associate Fellow.
‡Aerospace Engineer, Aerothermodynamics Branch, Aero- and Gas-Dynamics Division, Senior Member AIAA.
§Aerospace Engineer, Vehicle Analysis Branch, Space Systems and Concepts Division, Senior Member AIAA.

NOMENCLATURE

a	=	acceleration
C_A	=	axial force coefficient
C_D	=	drag coefficient
C_H	=	heat transfer coefficient
C_i	=	mass fraction of species i
C_L	=	lift coefficient
C_N	=	normal force coefficient
$C_{m,cg}$	=	pitching moment coefficient about center of gravity
DSMC	=	direct simulation Monte Carlo
d	=	maximum probe diameter
Kn	=	Knudsen number
p	=	pressure
q	=	heat transfer rate
R_a	=	afterbody radius
R_b	=	maximum probe radial dimension
R_c	=	corner radius
R_n	=	nose radius
T	=	temperature
V	=	freestream velocity
VHS	=	variable hard sphere
X_i	=	mole fraction of species i
x	=	axial distance from stagnation point measured along symmetry axis
x_{cp}	=	center of pressure location
y	=	radial distance from symmetry axis
α	=	angle of attack
γ	=	ratio of specific heats
λ	=	mean free path
ρ	=	density

Subscripts

cg	=	center of gravity
cp	=	center of pressure

w	=	surface values
∞	=	freestream values
HS	=	hard sphere

INTRODUCTION

Twenty-one years after two Viking spacecraft successfully landed on Mars (July 20, 1976 for Viking Lander I and Sept. 3 for Viking Lander II), Mars Pathfinder made a successful entry, descent, and landing July 4, 1997, thereby, achieving its primary objective[1] of demonstrating the use of a low-cost yet reliable system for landing on Mars. This system utilized four deceleration mechanisms (aeroshell, parachute, solid-rockets, and airbags) to slow Pathfinder's interplanetary approach velocity to zero after numerous bounces on the Mars surface in the Ares Vallis landing site.

Pathfinder has initiated a new era of Mars exploration that will involve multiple launches approximately every twenty-six months, and extending into the next decade. Pathfinder's configuration, a 70-deg half angle spherically blunted cone forebody and a conical frustum afterbody, along with its aerodynamic database has borrowed heavily on the Viking experience, and future Mars missions will leverage from the Pathfinder experience. An engineering objective of Pathfinder was the acquisition and return of data on the entry, descent, and landing system. Braun[1] et al. provide a post-entry overview of the approach navigation and atmospheric entry activities that supported Pathfinder's entry, descent, and landing operations.

The present paper is a continuation of the work of Moss[2] et al. concerned with the rarefied entry phase of Pathfinder as it enters the outer fringes of the Mars CO_2/N_2 atmosphere at a relative velocity of about 7.5 km/s and descends to freestream densities where hypersonic continuum flow conditions are encountered. Because of Pathfinder's center of gravity location, it is statically unstable for the free molecular and much of the transitional flow regime; that is, the flow regime bounded by free molecular and continuum flow. Consequently, rarefied aerodynamics is a significant issue for this entry capsule. This is particularly true for capsules without an active control system as is the case for Pathfinder and for the Stardust Sample Return Capsule[3,4].

The focus of this paper is on the aerodynamic database that has been generated using direct simulation Monte Carlo (DSMC) codes for the rarefied transitional flow regime. Results are presented of recent calculations[5] for Viking I entry that enhance the credibility of the current calculations for Pathfinder. In addition, results are presented that use the current data along with the flight acceleration measurements as part of the atmospheric reconstruction activity. The final results presented concern an examination of the consistency of the inferred spacecraft attitude during entry with that obtained from numerical simulations using a six-degree-of-freedom (DOF) analysis[6,7] that includes the present rarefied aerodynamic database.

Part of the aerodynamic database presented herein was included in Ref. 2 along with details concerning the flowfield structure, particularly the chemical reactions, and surface heating during the rarefied portion of entry. In the current paper, the aerodynamic database has been expanded to include additional angles of attack as well as lower Knudsen number conditions. Also, the consistency of the present calculations with the highest altitude Navier-Stokes calculations of Gnoffo[8] is demonstrated. The trends of the two data sets, rarefied and continuum, are shown to be consistent at nonzero incidence where overlap is not achieved and to achieve excellent agreement for zero incidence where overlap is achieved.

A best estimated trajectory for Pathfinder has been developed based on information along with an extensive aerodynamic database, including the current data for the rarefied transitional flow, and Pathfinder's acceleration data to establish the spacecraft attitude and Mars' atmospheric state properties[9,10] (density, pressure, and temperature). Results concerning the atmospheric reconstruction for density and Pathfinder's attitude during the rarefied flow regime are presented.

COMPUTATIONAL METHODS AND PHYSICAL MODELS

The computational tools utilized consisted of two DSMC codes complemented with a free molecular/Newtonian code. The G2 code of Bird[11,12], a 2D/axisymmetric code, was used to provide zero incidence DSMC calculations. G2 utilizes a body-fitted grid and has an extensive history of application and validation. For a G2 simulation, the computational domain can be subdivided into an arbitrary number of unstructured regions, each region further subdivided into

structured but variable size cells, and the cells subdivided into subcells to promote nearest neighbor collisions.

The 3D DSMC calculations were made using the code of LeBeau (described in Ref. 13) named DAC (DSMC Analysis Code). DAC uses a variable-resolution Cartesian grid currently consisting of two levels of cells. The resolution of the first level of cells is constant and is typically set based on the minimum desired flowfield resolution for a given problem. To further refine the flowfield grid in areas of increased density or high gradients, each level-1 cell can have an additional level of embedded Cartesian refinement. This second level of refinement is independent for each level-1 cell. The ability to refine the flowfield grid locally enhances DAC's ability to meet the spatial resolution required without excessive global refinement. The surface geometry for DAC is specified as a collection of planar triangular elements which form an unstructured triangular grid. The surface grid is defined independently of the volume grid. The reduced volumes of Cartesian cells that are clipped by the surface are computed and, to minimize the computational effort required to determine molecule-surface interactions, the surface triangles are mapped to the Cartesian cells. Uncoupling the surface and volume grids is a desirable feature when calculating aerodynamic moments particularly for highly rarefied flows in that the surface discretization can be resolved sufficiently to achieve accurate moment calculations without unnecessary flowfield resolution. More details concerning DAC features and capabilities are included in Refs. 13–14. An example of the good agreement between G2 and DAC for blunt body aerodynamics is discussed in Ref. 15 where the rarefied aerodynamics for the Galileo Probe (45.14° spherically blunted forebody with a hemispherical afterbody and a maximum diameter of 1.265 m) were calculated.

Free molecular and Newtonian values presented herein were calculated using the DACFREE code. This code was written by Wilmoth utilizing free molecular[12] and modified Newtonian[16] analytical expressions. An unstructured triangular surface grid is used to define the surface geometry, the same as used to define the surface geometry in DAC.

For both DSMC codes, the physical models are common. Molecular collisions are simulated using the variable hard sphere (VHS)[12] molecular model. Energy exchange between kinetic and internal modes is controlled by the Larsen-Borgnakke[17] statistical model. A rotational relaxation collision number of 5 and a vibrational collision number of 50 were used. Solutions were obtained with and without chemical reactions for a constant freestream gas composition consisting of 97 percent CO_2 and 3 percent N_2 by mass. Parameters used to define the VHS model were a reference temperature of 3000 K and a temperature exponent of viscosity of 0.8066.

For the calculations made with a reacting chemistry model, an updated version of the reaction set (54 reactions) utilized in the study by Hash and Hassan[18] was employed. This model consisted of eight species (O_2, N_2, O, N, NO, C, CO, and CO_2) while accounting for dissociation (40) and exchange (14) reactions.

The surface boundary conditions assumed the gas-surface interaction to be diffuse with full thermal accommodation to a specified surface temperature. For those calculations with reacting chemistry, the surface was assumed to be noncatalytic.

Representative examples of DSMC validation for blunt body hypersonic flows are given in Refs. 5, 19, and 20 where the test cases are closely related to the Pathfinder configuration. Several examples of applications of the G2 code of Bird to simulate ground based experiments performed as part of the AGARD Working Group 18 activity are included in Refs. 19 and 20. These test cases span a range of conditions (nonreacting to reacting flows) in the transitional to continuum regime. Comparisons of measurements and computations include flowfield structure, surface quantities and aerodynamics. In general, the G2 results were in good agreement with the measurements. Also, of direct relevance is the study of Blanchard et al.[5] where very good agreement for the normal-to-axial force ratio is achieved between the measured Viking I data and the DSMC simulations of the Viking spacecraft at 11 deg angle of incidence using the DAC code. Additional discussion of these data are presented later in the paper.

RESULTS AND DISCUSSION

A discussion of conditions, computational tools, and their implementation to generate an extensive aerodynamic database relevant to the rarefied flow entry regime experienced by Mars Pathfinder is presented. These data have direct relevance for the Mars '98 Lander entry capsule and for both the entry and aerocapture capsules for the Mars 2001 Lander and Orbiter missions. Each of these three capsules will utilize a 70-deg spherically blunted aeroshell, the configuration used for Pathfinder. Following the aerodynamics section is a discussion of the application of these data with flight measurements

from three-axis accelerometers to establish the attitude of Pathfinder during the rarefied flight regime and the atmospheric reconstruction to determine the density.

Mars Pathfinder Aerodynamic Calculations

The Pathfinder geometry and associated dimensions used in the present flowfield calculations are given in Fig. 1(a). The pre-flight freestream conditions listed in Table 1 were generated for a nominal entry trajectory using a Clancy[21] model for the Mars atmosphere. Note that the altitude parameter is de-emphasized in the present study since density (or equivalently, the Knudsen number as used herein) and velocity are the key parameters for the present study. For orientation, the altitude range for the present DSMC calculations is approximately 140 to 60 km. The best estimate of the actual Mars Pathfinder entry trajectory is illustrated in Fig. 1(b) where values for relative velocity, deceleration, and altitude are presented. The entry interface conditions (defined at a radius of 3522.2 km) for relative velocity and relative flight path angle were 7.470 km/s and −13.649 deg, respectively.

The calculations are initiated at a freestream density that corresponds to a hard sphere Knudsen number, $Kn_{\infty,HS}$, of 100. The hard sphere Knudsen number values are listed since most bridging relations used in trajectory analyses are based on hard sphere values. A constant molecular diameter of 4.64×10^{-10} m is assumed for the CO_2/N_2 gas. Consequently, the Knudsen number is the inverse of the freestream density defined as $Kn_{\infty,HS} = 2.8351\times10^{-8}/\rho_\infty$

Free Molecular Results Results for the free molecular aerodynamics are presented in Figs. 2 and 3 where the calculations were made using the DACFREE code. Freestream conditions are those for a Knudsen number of 100 and a wall temperature of 300 K. Shown are the center of pressure (Fig. 2) and the moment coefficient (Fig. 3) about the center of gravity (located 0.7154 m from the forebody nose) as a function of angle of incidence. The reference aerodynamic area and length are $\pi d_2/4$ and d, respectively, where d = 2.64927 m. The center of pressure location (Fig. 2) is approximately constant until the angle of attack approaches the afterbody angle (46.6°). When this occurs, the afterbody conical frustrum is no longer fully shadowed by the forebody and the center of pressure location moves aft until an angle of attack of about 90° is achieved. As α increases beyond 90°, the center of pressure moves forward as more of the afterbody sees the flow. At 133.4°, all the afterbody conical frustrum sees the flow and the center of pressure remains essentially constant for α up to 180°.

As shown in Figs. 2 and 3, with Pathfinder's center of mass location (0.7154 m from the nose), it is statically unstable at free molecular conditions except in a backward position for Mars entry. The modified Newtonian pitching moment results are also included in Fig. 3 where they were evaluated at freestream conditions corresponding to a Knudsen number of 0.001 (continuum flow) and with a ratio of specific heats equal 1.2 (value selected such that the stagnation pressure coefficient at zero incidence agrees with the DSMC results of 1.91). As evident in Fig. 3, Pathfinder goes from a statically unstable condition to a statically stable condition as it traverses the transitional flow regime with the frictional forces (more significant in the rarefied regime) being the destabilizing source. The impact on the entry attitude profile depends on how deep in the transitional flow regime the instability persists and the attitude control option exercised. As will be discussed later [see Fig. 5(d)], the static instability persists to a Knudsen number between 0.1 and 0.2 where the zero incidence forces have increased from 0.09 N at $Kn_{\infty,HS}$ = 100 to 93.7 N at $Kn_{\infty,HS}$ = 0.109 (7027 N at $Kn_{\infty,HS}$ = 0.001). Unlike the Viking I and II capsules which utilized an active control system throughout their entries, Mars Pathfinder did not rely on any form of active control (Ref. 6). Instead, an initial spin of two revolutions per minute and aerodynamic damping were utilized to provide vehicle stability throughout the entire atmospheric flight.

Axisymmetric calculations using G2 Calculations were made for all of the freestream conditions listed in Table 1 using the G2 DSMC code with the reacting chemistry model described earlier. The results reported by Moss[2] et al. for these conditions contained two errors in the chemistry model. In the present study, the calculations have been repeated with the chemistry model corrections, and the calculations show a negligible effect on aerodynamics and less than 10 percent effect on stagnation heating. For these calculations, the computational domain included only the Pathfinder forebody up to the maximum body diameter, location 3 in Fig. 1. A solution including the afterbody for a Knudsen number of 0.0036 is discussed in Ref. 2. Common to all the calculations was the subdivision of the forebody computational domain into four arbitrary regions and the use of 62 cells along the

forebody surface. The size of the computational domain, the number of cell divisions normal to the surface, and the geometric progression of the cell size were adjusted with rarefaction to ensure that the cell size normal to the surface was less than the local mean free path length. Also, each cell was subdivided into 4 subcells. The number of molecules used in these simulations range from 76,000 to 290,000.

Included in Table 1 are values for drag coefficient, C_D, stagnation-point heat transfer coefficient $\left(C_H = 2q/\rho_\infty V_\infty^3\right)$ and stagnation-point heating results. Figure 4 presents the drag coefficient as a function of hard-sphere Knudsen number, effectively the inverse of the freestream density. Evident is the increase in the drag coefficient (equivalent to C_A for $\alpha = 0°$) as the flow rarefaction increases from continuum to free molecular conditions, approaching the free molecular value of 2.072 for an assumed wall temperature of 300 K. Note that free molecular conditions occur at a Knudsen number higher than 100 based on the drag coefficient results. In this figure, the free molecular result is arbitrarily placed at Knudsen number 1000. For the range of conditions considered, the frictional drag component increases from 0.6 percent of the total drag at $Kn_{\infty,HS} = 0.001$ to 13.2 percent at a $Kn_{\infty,HS} = 100$. Also shown are results of two Navier-Stokes (NS) solutions, again for only the forebody, obtained by Gnoffo[8] (included in Table 2) using the Langley Aerothermodynamic Upwind Relaxation Algorithm (LAURA) code. Agreement between the DSMC and NS solutions is very good. The calculations of Gnoffo show that the Pathfinder drag coefficient at $\alpha = 0°$ continues to increase in the hypersonic continuum regime until a value of $C_D = 1.718$ is reached at a velocity of about 4.5 km/s.

Three dimensional calculations using DAC The matrix of 3-D solutions that have been generated with DAC consisted of angles of attack of 0° to 30° and Knudsen numbers between 100 and 0.027. As will become evident later, angles of attack of 5 deg or less are relevant to Pathfinder's entry. The computational results presented are for a non-reacting CO_2/N_2 gas model that had active vibrational and rotational modes (not a calorically perfect gas). While completing the 3D computations, a reacting CO_2/N_2 gas model was implemented for DAC having the same data as used for G2 code. Comparisons of DAC and G2 results for surface heating and chemical species distributions showed excellent agreement, indicating consistent results for the two codes.

As discussed in Ref. 2, blunt body aerodynamics for hypersonic rarefied flows seem to be insensitive to whether the simulation is made with a reacting or non-reacting gas model, provided the vibrational modes are active. In the current study, several solutions were made with DAC using the reacting chemistry model for 5-deg angle of incidence. The reacting results showed good agreement with the non-reacting simulations; consequently, all results presented for DAC are for the two species non-reacting gas model.

Axial, normal, moment, drag, and lift coefficients are tabulated in Table 2. The tabulated moment coefficients, $C_{m,cg}$, are with respect to Pathfinder's center of gravity located 0.7154 m from the nose. The numerical simulations utilized the symmetry of the problem in that the flow is computed about half of the capsule only. The forebody and near wake are included in the computational domain. At the more rarefied conditions only level-one cells are used in the simulations. For Knudsen numbers of 0.404 and less, a minimum of two solutions were generated for each matrix point: a solution using a constant level-1 cell resolution throughout the computational domain was obtained and then at least one grid adaption was made to arrive at a new grid, where each level-1 cell has an independent refinement based on the local conditions within the level-1 cells. For the 0.404 Knudsen number condition, the impact on the calculated results was a reduction of about 1.5 percent in C_A. For the higher density conditions, the grid refinement produced a more significant reduction in the aerodynamic coefficients and the results listed in Table 2 are based on the refined grid. The maximum number of particles used in the present 3-D simulations was 2.8 million.

When the DAC results for C_A at $\alpha = 0°$ are compared with the G2 results (Fig. 4), the agreement is very good (better than 1.0 percent) except for the lower Knudsen number DAC calculations. This difference is believed to be due to inadequate grid resolution near the surface in the present DAC simulation (cell sizes for the two smallest Knudsen number solutions were at best 2.5 times and 8.0 times, respectively, the local mean free path along the forebody surface). Even at the lowest Knudsen number conditions, the differences in results are less than 2 percent; however, the normal (see Fig. 9) and moment coefficients for nonzero angle of attack are more sensitive to grid resolution than the axial

coefficient as has been demonstrated by Gnoffo[8] for continuum calculations. Use of larger computational resources could resolve this question.

Figures 5(a) through 5(h) present the 3-D results for the aerodynamic coefficients as a function of angle of attack and rarefaction. As shown in Ref. 2 the free molecular values using DACFREE are in excellent agreement with DAC when the collisions are deactivated (collisionless DSMC). Also, the magnitude of $Kn_{\infty,HS}$ is of the order of 100 or greater before free molecular conditions are achieved. These calculations show that Pathfinder becomes statically stable at small angles of attack for $Kn_{\infty,HS}$ of the order 0.1 [Fig. 5(d)]. The aft movement of the center of pressure [Fig. 5(h)] is shown to be insensitive to angle of attack variations less than 15°. The lift [Fig. 5(f)] is negative and quite small in comparison to the drag [Fig. 5(e)] for most of the transitional regime. Also included in Fig. 5 and Table 2 are the Navier-Stokes results of Gnoffo[8] obtained with the LAURA code for Knudsen numbers that are one and two orders of magnitude smaller than the DAC results. The DAC and LAURA data shown in Fig. 5 provide aerodynamic data from free molecular to well into the continuum flow regime. Gnoffo's results for $Kn_{\infty,HS} = 0.0003$ indicate that Pathfinder is statically unstable for this flow condition at small angles of incidence. As discussed by Gnoffo[8], this behavior occurs in the continuum regime due to the changing chemical state of the shock layer (producing sonic line movement) with entry conditions.

The study of Blanchard[5] et al. provided additional reinforcement that the current DSMC codes provide reliable aerodynamic characteristics for rarefied hypersonic flight regimes, particularly for Mars entries. Figures 6 and 7 are extracted from Ref. 5 and show a comparison of DAC results for aerodynamic coefficients with flight measured results for the Viking I entry. The Viking entries were from orbit rather than a direct entry, hence a lower entry velocity (4.5 km/s) than Pathfinder but with the same forebody shape (a 70-day spherically blunted cone) and a larger base diameter (equal to 3.5 m). The attitude control system for Viking maintained an angle of attack of 11 deg (measured with gyros) during the rarefied portion of entry. Results for normal-to-axial force ratios are in excellent agreement (Fig. 6) where the noise-to-signal ratio of the measurements become large at the larger Knudsen number conditions. Also, the calculated drag coefficient (Fig. 7) has the correct qualitative behavior as it approaches the measured continuum results (stagnation pressure measurements used[22] to separate the drag coefficient from density).

Flight Measurements and Reconstruction

Since the July 4 landing, a goal of the Mars Pathfinder team was to determine the performance of Pathfinder's entry, descent, and landing systems. This requires the reconstruction of the Mars atmospheric structure at the time of entry. Density profile accuracy depends critically on C_A knowledge while the spacecraft attitude can be inferred from acceleration measurements and accurate knowledge concerning C_N/C_A ratio. Data presented in Tables 1 and 2 are essential elements in the overall aerodynamic database that has been utilized in the postflight analyses.

Utilization of Measurements and Computations

During Pathfinder's hypersonic entry, the only measurements made were that of acceleration. For the two Viking entries, additional data were available from gyros (providing angle of incidence), mass spectrometer (rarefied data), and stagnation pressure (continuum data) measurements. The latter two measurements provided data for determination of atmospheric density and aerodynamic coefficients. With Pathfinder's more limited suite of measurements, explicit dependence on an aerodynamic database appropriate for the spacecraft configuration and entry conditions is required to establish the vehicle's attitude and the freestream atmospheric state properties during entry. Such a procedure is described in Refs. 9 and 10. Here, a best estimated trajectory is first established independent of aerodynamics and atmospheric predictions by integrating the accelerometer data directly. With knowledge concerning this trajectory, three-axis acceleration measurements, and an appropriate aerodynamic database, one can establish the angle of incidence and density by an iterative procedure. With the aerodynamic coefficients available from an existing database as a function of flow conditions, the angle of incidence and freestream density are calculated. This process is repeated until the assumed and calculated freestream conditions converge. The results of such a procedure applied to Pathfinder's entry are presented in Figs. 8 through 11. Figure 8 presents measured normal-to-axial force (acceleration) ratio data for Pathfinder as a function of freestream density and Knudsen number. The normal acceleration is the vector sum of the two acceleration components in the plane normal to the axial direction. For densities less than 10^{-7} kg/m^3,

the normal accelerations are less than the resolution of the accelerometers. Pathfinder had a total of six accelerometers, three engineering and three science accelerometers. The data used herein is taken from the science accelerometers since they were mutually orthogonal, oriented parallel to the spacecraft axes, and were range switched during entry. Each accelerometer signal channel had three gain states, giving dynamic ranges of ±40 g, ±800 mg, and ±16 mg. Signals for the axial accelerometer were digitized to 14 bits to provide 5 mg, 100 μg, and 2 μg resolution, respectively. Signals for the two accelerometers normal to the axial accelerometer were digitized to only 8 bits, hence a lower resolution by a factor of 64. The decreasing magnitude of C_N/C_A with increasing atmospheric density is due to two factors; one is that the normal to axial force decreases with decreasing rarefaction [Fig. 5(c)] and two that the angle of incidence is decreasing as discussed later.

Figure 9 presents the corresponding calculated normal-to-axial force (acceleration) ratio data as a function of freestream density and Knudsen number for several angles of incidence. When the two data sets are utilized in the atmospheric reconstruction process, one sees (Fig. 10) that the inferred angles of incidence are quite small (less than 3.0 deg) for that portion of the transitional flow regime where both normal and axial acceleration data are available ($Kn_{\infty,HS} < 0.3$). Furthermore, the angle of incidence approaches zero with increasing density, then experiences substantial fluctuations in magnitude after a range switch from ±16mg to ±800mg is executed for the axial accelerometer. These fluctuations are not associated with the axial accelerometer range change since they occur at a sufficient time after this instrument event. The actual source of the fluctuations, present in the data for each of the three accelerometers, is not known. However, a possible mechanism is the asymmetric removal of a single layer of double aluminized Kapton that encapsulated the forbody heat shield. This 1-mil thick Kapton layer was used to provide thermal control during the seven month cruise phase of the mission and was designed to be removed at some point during the entry phase of the mission by the aerothermal entry environment. At higher densities (Knudsen number of about 0.0017), a range switch is made from ±800 mg to ±40 g. After initial data fluctuations, there is a fluctuating but increasing angle of incidence observed in the continuum flow region that is indicative of the first continuum static instability that occurs for small angles of incidence as discussed by Gnoffo[8]. For more rarefied conditions ($Kn_{\infty,HS} > 0.3$), additional modeling[9] has been used to infer the angle of incidence.

With knowledge of the angle of incidence for a given flow condition, the reconstructed density (Fig. 11) is a direct calculation using the following relations:

$$\text{Axial acceleration} = \text{Axial force/mass} = C_A * \left(0.5 * \rho_\infty * V_\infty^2 * A\right) / \text{mass}.$$

With velocity known from the trajectory reconstruction, the spacecraft cross sectional area, A, of 5.51242 m^2, and the spacecraft mass assumed to be constant at 585.3 kg, the freestream density is determined using the calculated axial force coefficient appropriate for the freestream conditions. Data for the reconstructed density presented in Fig. 11 are from the onset of detectable axial deceleration to parachute deployment. Aerodynamic data for free molecular and transitional flow is that reported herein while the continuum data is that presented by Gnoffo[8]. Denoted in Fig. 11 are the density conditions for the current DSMC calculations.

The Pathfinder atmospheric density profile when compared with Viking I data[5] show a more tenuous atmosphere at the higher altitudes by factors of three to four. The Clancy[21] atmospheric model used in the current calculations is in much closer agreement with Pathfinder's experience than that of Viking I. Data from the recent experience of the Mars Global Surveyor, undergoing aerobraking at minimum altitudes of about 120 km, have shown density variations as large as a factor of two on succeeding orbit passes. This is indicative of the large high-altitude atmospheric density variations that can occur at Mars over a relatively short time interval.

Consistency of Measurements and Computations

As evident from the previous discussion, the acceleration measurements and numerical calculations/simulations used to infer vehicle attitude and atmospheric density do not provide a direct validation of the computational tools since the results of the computations were an essential part of the reconstruction process. However, the overall consistency of what is inferred from flight with that generated from a six-DOF aerodynamic database is instructive, even though more modeling issues[6] are involved such as the Mars atmospheric and gravitational models.

Results of a six-DOF trajectory simulations for Pathfinder's entry are presented in Figs. 12 and 13

where the calculated angle of incidence is shown as a function of both time and density. This same six-DOF simulation was used during the design, test, and operations phase of the Pathfinder mission[1]. This simulation utilized the current aerodynamic database and is initiated at a density of 5.0×10^{-10} which corresponds to an altitude of about 132 km. Also, the entry attitude of the vehicle was assumed to be at 2-deg incidence. Results of the trajectory simulation for vehicle attitude are in good agreement with the flight inferred results in that both sets of data show the total angle of incidence is less than 5 deg from the onset of the normal-to-axial acceleration measurements (approximately 21 s as shown in Fig. 12 where $\rho_\infty = 1.0\times10^{-7}$ kg/m^3) to parachute deployment. Figure 13 shows a comparison of flight inferred and six-DOF results as a function of freestream density for that portion of the transitional flow regime where measurements were obtained. Results of the trajectory simulation for vehicle attitude are in qualitative agreement with the flight inferred results in that the initial angle of incidence is decreasing with increasing density for values of density greater than 1×10^{-7} kg/m^3, the smallest value for which measurements could be inferred from acceleration data. However, the six-DOF simulation shows a somewhat larger angle of incidence in the rarefied regime when compared with the flight inferred results. The source of this inconsistency is presently unknown and difficult to resolve with Pathfinder's limited suite of instruments. Inclusion of gyros as part of the flight instrumentation is very desirable for future Mars missions.

Although the vehicle is statically unstable for densities less than 2×10^{-7} kg/m^3 ($Kn_{\infty,HS} > 0.1$), the gyroscopic stability caused by Pathfinder's 2 rpm spin initially overwhelms this aerodynamic moment. During this period of atmospheric flight, the vehicle's flight-path angle is also becoming more shallow. In fact, this parameter decreases by approximately 1.5 degrees as the density increases from 1×10^{-10} kg/m^3 to 1×10^{-7}kg/m^3. As shown in Fig. 14, since the Pathfinder flight vehicle is gyroscopically stiff, this change in flight-path angle induces an increase in angle of attack from 2.0 to approximately 3.5 degrees. To further illustrate the impact of Pathfinder's 2 rpm spin rate on vehicle attitude, a six-degree-of-freedom simulation was performed with no spin. This data is also shown in Fig. 14. For this case, where the vehicle has no gyroscopic stability, the vehicle initially follows the velocity vector as the flight-path angle shallows. Although the vehicle is statically unstable in this region of the atmospheric flight (density < 7×10^{-8} kg/m^3), the aerodynamic moment is simply too small to impact the initial vehicle attitude. As a result a near-constant 2 degree angle-of-attack results. However, as the density continues to increase, the significance of the transitional regime static instability grows, causing the vehicle's angle-of-attack to increase as high as 4.5 degrees. Hence, while the Pathfinder entry vehicle is statically unstable in the free-molecular and for much of the transitional flow regime, the vehicle's 2 rpm spin rate was able to counter this small destabilizing aerodynamic moment.

CONCLUDING REMARKS

Direct simulation Monte Carlo (DSMC) calculations have been used to generate an aerodynamic database applicable to the rarefied portion of the Mars Pathfinder's entry as well as for future Mars missions. The current database is being utilized in ongoing atmospheric reconstruction studies and results are presented for the density reconstruction and spacecraft attitude determination based on flight accelerometer data and computed axial and normal aerodynamic coefficients.

Recent 3-D DSMC calculations for the Mars Viking I spacecraft aerodynamics show excellent agreement with flight measured results. These results provide additional confidence in the credibility of these codes to predict accurate aerodynamics for Mars missions. In the current calculations for Pathfinder, the computed results are shown to be consistent with Navier-Stokes results for zero incidence conditions where overlap was achieved and to provide consistent qualitative trends for the 3-D calculations where overlap was not achieved.

When the current aerodynamic database is incorporated in a six-degree-of-freedom trajectory simulation, the results of the simulation are in qualitative agreement with the trends observed for the flight inferred spacecraft attitude. However, the magnitude of the angles in the transitional flow regime are greater for the trajectory simulation than that for the flight inferred data. Additional instrumentation planned for flight on the Mars '98 and '01 missions should help resolve this minor inconsistency.

REFERENCES

[1]Braun, R. D., Spencer, D. A., Kallemeyn, P. A., and Vaughan, R. M., "Mars Pathfinder Atmospheric Entry Navigation Operations", AIAA Paper 97-3663, August 1997.

[2]Moss, J. N., Wilmoth, R. G., and Price, J. M., "DSMC Simulations of Blunt Body Flows for Mars Entries: Mars Pathfinder and Mars Microprobe Capsules", AIAA Paper 97-2508, June 1997.

[3]Wilmoth, R. G., Mitcheltree, R. A., and Moss, J. N., "Low-Density Aerodynamics of the Stardust Sample Return Capsule", AIAA Paper 97-2510, June 1997.

[4]Desai, P. N., Mitcheltree, R. A., and Cheatwood, F. M., "Entry Dispersion Analysis for the Stardust Comet Sample Return Capsule," AIAA Paper 97-3012, August 1997.

[5]Blanchard, R. C., Wilmoth, R. G., and Moss, J. N., "Aerodynamic Flight Measurements and Rarefied-Flow Simulations of Mars Entry Vehicles", *Journal of Spacecraft and Rockets*, Vol. 34, No. 5, Sept–Oct 1997, pp. 687–690.

[6]Braun, Robert D., Powell, Richard W., Engelund, Walter C., Gnoffo, Peter A., Weilmuenster, K. James, and Mitcheltree, Robert A., "Mars Pathfinder Six-Degrees-of-Freedom Entry Analysis," *Journal of Spacecraft and Rockets*, Vol. 32, No. 6, Nov–Dec 1995, pp. 993–1000.

[7]Brauer, G., Cornick, D., and Stevenson, R., "Capabilities and Applications of the Program to Optimize Simulated Trajectories (POST)," NASA CR-2770, Feb. 1977.

[8]Gnoffo, P. A., Weilmuenster, K. J., Braun, R. D., and Cruz, C. I., "Influence of Sonic-Line Location on Mars Pathfinder Probe Aerodynamics," *Journal of Spacecraft and Rockets*, Vol. 33, No. 2, March–April 1996, pp. 169–177.

[9]Blanchard, R. C., Spencer, D. A., and Braun, R. D., "Pathfinder Entry Trajectory and Atmosphere Reconstruction", To be published, 1998.

[10]Spencer, D. A., Blanchard, R. C., Braun, R. D., and Thurman, S. W., "Mars Pathfinder Atmospheric Entry Reconstruction," AAS/AIAA Spaceflight Mechanics Conference, Monterey, CA, Feb. 1998.

[11]Bird, G. A., *"The G2/A3 Program Users Manual."* G. A. B. Consulting Pty Ltd, Killara, N.S.W., Australia, March 1992.

[12]Bird, G. A., *"Molecular Gas Dynamics and the Direct Simulation of Gas Flows,"* Clarendon Press, Oxford, 1994.

[13]Wilmoth, R. G., LeBeau, G. J., and Carlson, A. B., "DSMC Grid Methodologies for Computing Low-Density Hypersonic Flows about Reusable Launch Vehicles," AIAA Paper 96-1812, June 1996.

[14]LeBeau, G. J. and Wilmoth, R. G., "Application of the DAC DSMC Code to a Variety of Three Dimensional Rarefied Gas Dynamics Problems", Abstract submitted to the 21st International Symposium on Rarefied Gas Dynamics, Marseille, France, July 26–31, 1998.

[15]Moss, James N., LeBeau, Gerald J., Blanchard, Robert C., and Price, Joseph M., "Rarefaction Effects on Galileo Probe Aerodynamics," *Rarefied Gas Dynamics 20*, edited by Ching Shen, Peking Univ. Press, Beijing, China, 1997, pp. 495–500.

[16]Anderson, J. D., Jr., *"Hypersonic and High Temperature Gas Dynamics,"* McGraw-Hill Book Company, 1989.

[17]Borgnakke, C. and Larsen, P.S., "Statistical Collision Model for Monte Carlo Simulation of Polyatomic Gas Mixture," *Journal of Computational Physics*, Vol. 18, No. 4, 1975, pp. 405–420.

[18]Hash, David B. and Hassan, H. A., "Monte Carlo Simulation of Entry in the Martian Atmosphere," *Journal of Thermophysics and Heat Transfer*, Vol. 7, No. 2, April–June 1993, pp. 228–232.

[19]Anon, "Hypersonic Experimental and Computational Capabilities: Improvement and Validation," AGARD AR-319, Vol. 2, To be published in 1997.

[20]Moss, J. N. and Price, J. M., "Survey of Blunt Body Flows Including Wakes at Hypersonic Low-Density Conditions," *Journal of Thermophysics and Heat Transfer*, Vol. 11, No. 3, July–Sept 1997.

[21]Clancy, R. T., Lee, S. W., Gladstone, G. R., McMillan, W. W., and Rousch, T., "A New Model of Mars Atmospheric Dust Based on Analysis of Ultraviolet Through Infrared Observations for Mariner-9, Viking and Phobos," *Journal of Geophysical Research*, Vol. 100, 1995, pp. 5251–5263.

[22]Blanchard, R. C., and Walberg, G. D., "Determination of the Hypersonic-Continuum/ Rarefied-Flow Drag Coefficient of the Viking Lander Capsule I Aeroshell from Flight Data," NASA TP 1793, Dec. 1980.

Table 1. Conditions[a] and results[b] for Mars Pathfinder calculations

Condition	V_∞, m/s	ρ_∞, kg/m^3	T_w[c], K	$Kn_{\infty,HS}$	C_D	Stagnation Point Heating	
						C_H	q, W/cm^2
1	7,463.1	2.8351×10^{-10}	300	1.00×10^{2}	2.066	1.000	5.92×10^{-3}
2	7,463.1	1.1767×10^{-9}	389	2.41×10^{1}	2.059	0.981	2.40×10^{-2}
3	7,468.6	5.6344×10^{-9}	470	5.03×10^{0}	2.014	0.945	1.11×10^{-1}
4	7,472.8	1.8386×10^{-8}	560	1.54×10^{0}	1.972	0.861	3.30×10^{-1}
5	7,477.3	7.0212×10^{-8}	675	4.04×10^{-1}	1.915	0.801	1.18×10^{0}
6	7,479.5	1.3759×10^{-7}	750	2.06×10^{-1}	1.871	0.715	2.06×10^{0}
7	7,481.5	2.6074×10^{-7}	824	1.09×10^{-1}	1.834	0.700	3.82×10^{0}
8	7,483.3	5.1816×10^{-7}	900	5.47×10^{-2}	1.746	0.578	6.27×10^{0}
9	7,484.6	1.0342×10^{-6}	950	2.74×10^{-2}	1.687	0.418	9.06×10^{0}
10	7,484.6	2.0301×10^{-6}	1000	1.40×10^{-2}	1.657	0.269	1.14×10^{1}
11	7,453.9	7.9450×10^{-6}	1100	3.57×10^{-3}	1.666	0.094	1.54×10^{1}
12	7,431.3	2.7614×10^{-5}	1500	1.03×10^{-3}	1.681	0.035	1.96×10^{1}

[a]Freestream mole fractions are $X_{CO_2} = 0.9537$ and $X_{N_2} = 0.0463$, molecular weight = 43.2685, freestream temperature = 137.4 K, and diffuse surface with full thermal accommodation. Freestream density and temperature are from Clancy model[21].

[b]G2 results for zero incidence

[c]Assumed wall temperature values

Table 2. Calculated Aerodynamics for Mars Pathfinder

Angle of attack, deg	C_A	C_N	$C_{m,cg}$	C_D	C_L
		Free molecular results			
0	2.0723	0.0000	0.0000	2.0723	0.0000
2	2.0698	0.0699	0.0060	2.0710	–0.0024
5	2.0568	0.1740	0.0149	2.0641	–0.0059
10	2.0111	0.3428	0.0295	2.0401	–0.0116
15	1.9379	0.5017	0.0433	2.0017	–0.0169
20	1.8390	0.6462	0.0555	1.9491	–0.0218
25	1.7165	0.7718	0.0661	1.8818	–0.0260
30	1.5740	0.8749	0.0748	1.8006	–0.0293
		$Kn_{\infty,HS}$ = 100.0, DAC results			
0	2.0652	0.0000	0.0000	2.0652	0.0000
2	2.0622	0.0693	0.0059	2.0634	–0.0028
5	2.0487	0.1725	0.0148	2.0559	–0.0067
10	2.0047	0.3402	0.0285	2.0333	–0.0130
15	1.9307	0.4977	0.0421	1.9937	–0.0189
20	1.8333	0.6413	0.0543	1.9421	–0.0244
25	1.7134	0.7670	0.0638	1.8770	–0.0290
30	1.5731	0.8706	0.0721	1.7977	–0.0326

Table 2. Continued

Angle of attack, deg	C_A	C_N	$C_{m,cg}$	C_D	C_L
			$Kn_{\infty,HS}$ = 24.09, DAC results		
0	2.0510	0.0000	0.0000	2.0510	0.0000
2	2.0483	0.0676	0.0053	2.0494	−0.0039
5	2.0398	0.1690	0.0137	2.0468	−0.0095
10	1.9960	0.3336	0.0270	2.0236	−0.0181
15	1.9256	0.4880	0.0390	1.9863	−0.0270
20	1.8253	0.6275	0.0507	1.9298	−0.0346
25	1.7066	0.7505	0.0603	1.8639	−0.0410
30	1.5704	0.8533	0.0681	1.7867	−0.0462
			$Kn_{\infty,HS}$ = 5.03, DAC results		
0	1.9940	0.0000	0.0000	1.9940	0.0000
2	1.9922	0.0631	0.0044	1.9932	−0.0065
5	1.9867	0.1575	0.0118	1.9929	−0.0162
10	1.9445	0.3099	0.0228	1.9688	−0.0325
15	1.8779	0.4550	0.0337	1.9317	−0.0466
20	1.7811	0.5831	0.0424	1.8731	−0.0613
25	1.6699	0.6991	0.0504	1.8089	−0.0722
30	1.5393	0.7944	0.0568	1.7302	−0.0817
			$Kn_{\infty,HS}$ = 1.54, DAC results		
0	1.9688	0.0000	0.0000	1.9688	0.0000
2	1.9653	0.0580	0.0039	1.9661	−0.0107
5	1.9537	0.1442	0.0094	1.9588	−0.0267
10	1.9145	0.2842	0.0183	1.9348	−0.0525
15	1.8419	0.4146	0.0265	1.8864	−0.0762
20	1.7565	0.5362	0.0345	1.8340	−0.0969
25	1.6472	0.6415	0.0407	1.7640	−0.1148
30	1.5201	0.7293	0.0447	1.6811	−0.1285
			$Kn_{\infty,HS}$ = 0.404, DAC results		
0	1.9308	0.0000	0.0000	1.9308	0.0000
2	1.9277	0.0488	0.0023	1.9283	−0.0185
5	1.9193	0.1215	0.0059	1.9225	−0.0462
10	1.8834	0.2405	0.0106	1.8956	−0.0900
15	1.8125	0.3507	0.0150	1.8415	−0.1304
20	1.7286	0.4560	0.0185	1.7803	−0.1627
25	1.6242	0.5454	0.0215	1.7025	−0.1921
30	1.5025	0.6222	0.0232	1.6123	−0.2124

Table 2. Continued

Angle of attack, deg	C_A	C_N	$C_{m,cg}$	C_D	C_L
		$Kn_{\infty,HS}$ = 0.206, DAC results			
0	1.8830	0.0000	0.0000	1.8830	0.0000
2	1.8791	0.0421	0.0010	1.8794	–0.0236
5	1.8656	0.1037	0.0026	1.8675	–0.0593
10	1.8301	0.2070	0.0040	1.8382	–0.1139
15	1.7709	0.3037	0.0057	1.7892	–0.1650
20	1.6882	0.3937	0.0072	1.7211	–0.2074
25	1.5873	0.4740	0.0069	1.6389	–0.2412
30	1.4692	0.5425	0.0062	1.5436	–0.2647
		$Kn_{\infty,HS}$ = 0.109, DAC results			
0	1.8314	0.0000	0.0000	1.8314	0.0000
2	1.8256	0.0354	–0.0001	1.8257	–0.0283
5	1.8151	0.0873	–0.0004	1.8158	–0.0712
10	1.7814	0.1763	–0.0017	1.7849	–0.1357
15	1.7257	0.2592	–0.0021	1.7340	–0.1963
20	1.6409	0.3346	–0.0043	1.6564	–0.2468
25	1.5413	0.4042	–0.0073	1.5678	–0.2850
30	1.4261	0.4646	–0.0107	1.4673	–0.3107
		$Kn_{\infty,HS}$ = 0.055, DAC results			
0	1.7776	0.0000	0.0000	1.7776	0.0000
2	1.7774	0.0280	–0.0013	1.7773	–0.0341
5	1.7669	0.0695	–0.0027	1.7662	–0.0848
10	1.7315	0.1372	–0.0055	1.7290	–0.1656
15	1.6722	0.2047	–0.0092	1.6682	–0.2351
20	1.5734	0.2674	–0.0159	1.5700	–0.2869
25	1.4677	0.3209	–0.0221	1.4658	–0.3294
30	1.3542	0.3702	–0.0296	1.3579	–0.3566
		$Kn_{\infty,HS}$ = 0.027, DAC results			
0	1.7122	0.0000	0.0000	1.7122	0.0000
2	1.7106	0.0239	–0.0014	1.7104	–0.0358
5	1.6983	0.0589	–0.0033	1.6970	–0.0893
10	1.6658	0.1191	–0.0072	1.6612	–0.1719
15	1.6064	0.1768	–0.0122	1.5975	–0.2450

Table 2. Concluded

$Kn_{\infty,HS}$ = 0.0030, LAURA solutions of Gnoffo[8]					
0	1.6625	0.0000	0.0000	1.6625	0.0000
2	1.6597	0.0075	−0.0011	1.6590	−0.0504
5	1.6508	0.0185	−0.0024	1.6461	−0.1254
11	1.5767	0.0452	−0.0116	1.5690	−0.2590
$Kn_{\infty,HS}$ = 0.00030, LAURA solutions of Gnoffo[8]					
0	1.6768	0.0000	0.0000	1.6768	0.0000
2	1.6796	0.0036	−0.0001	1.6787	−0.0550
5	1.6595	0.0112	−0.0027	1.6542	−0.1335
11	1.5767	0.0359	−0.0172	1.5546	−0.2656

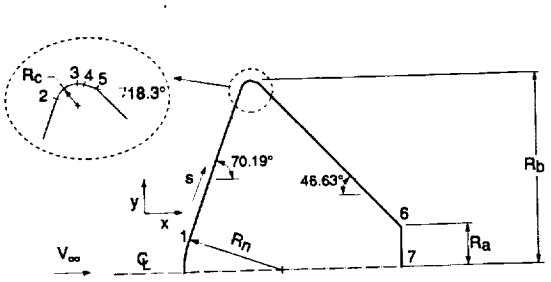

Location	x	y	s
1	0.0393	0.2250	0.2295
2	0.4196	1.2808	1.3518
3	0.4820	1.3246	1.4330
4	0.5028	1.3213	1.4541
5	0.5386	1.3094	1.4919
6	1.5059	0.2855	2.9000
7	1.5059	0.0000	3.1859

Dimensions in m

(a) Configuration (R_n = 0.6638, R_c = 0.0662, R_a = 0.2855 and R_b = 1.3246)

Fig. 1 Mars Pathfinder's configuration and trajectory characteristics.

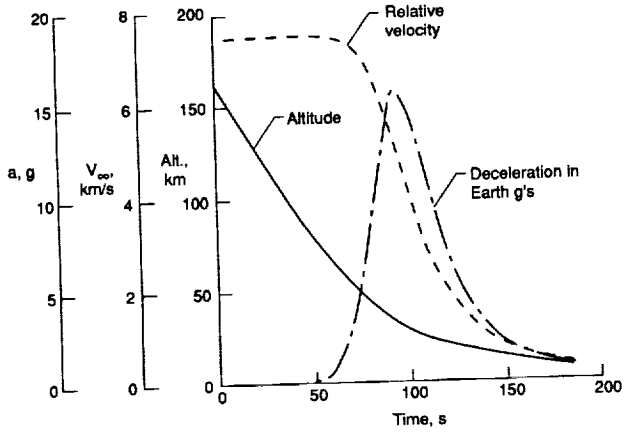

(b) Entry trajectory characteristics.

Fig. 1 Concluded.

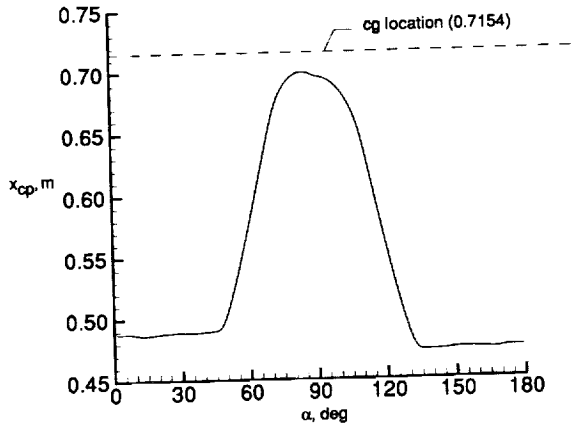

Fig. 2 Pathfinder free molecular center of pressure location as a function of angle of attack.

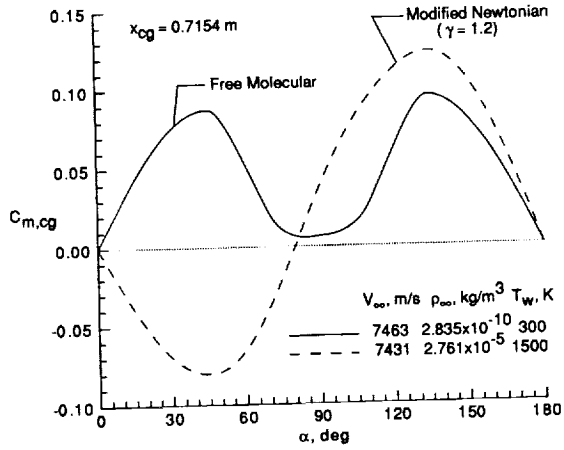

Fig. 3 Pathfinder pitching moment coefficient computed using free molecular and modified Newtonian (γ = 1.2) relations as a function of angle of attack.

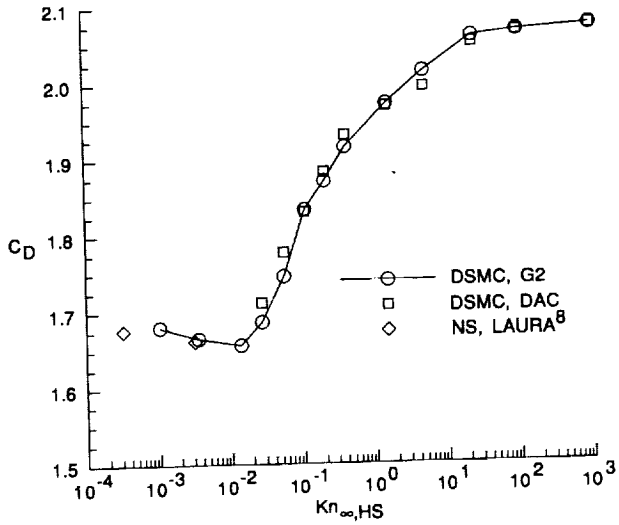

Fig. 4 Pathfinder drag coefficient at α = 0°.

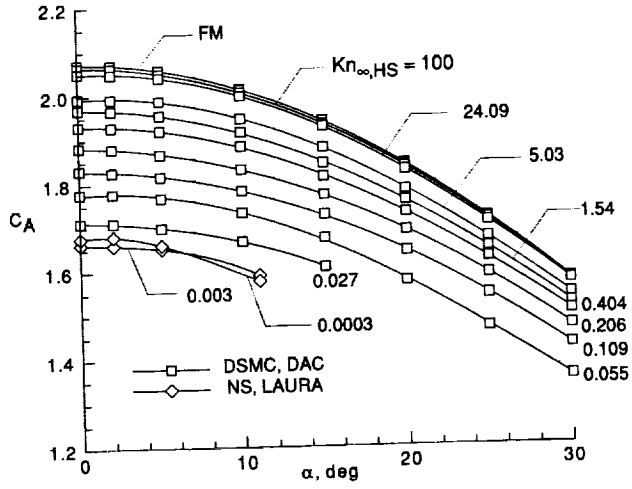

(a) Axial coefficient.

Fig. 5 Pathfinder aerodynamic coefficients as a function of angle of attack and rarefaction (LAURA results are those of Gnoffo[8]).

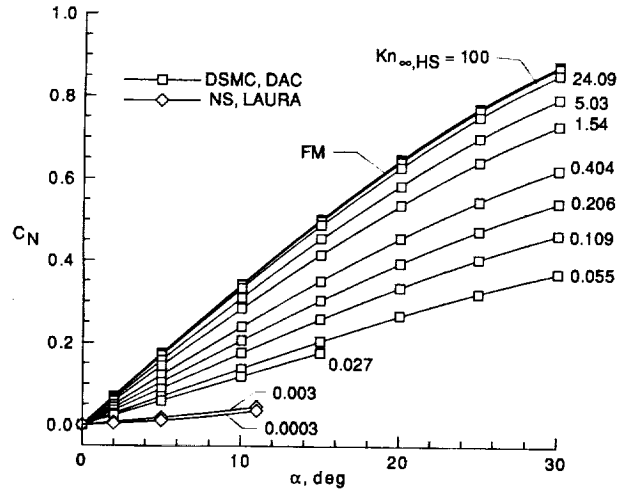

(b) Normal coefficient.
Fig. 5 Continued.

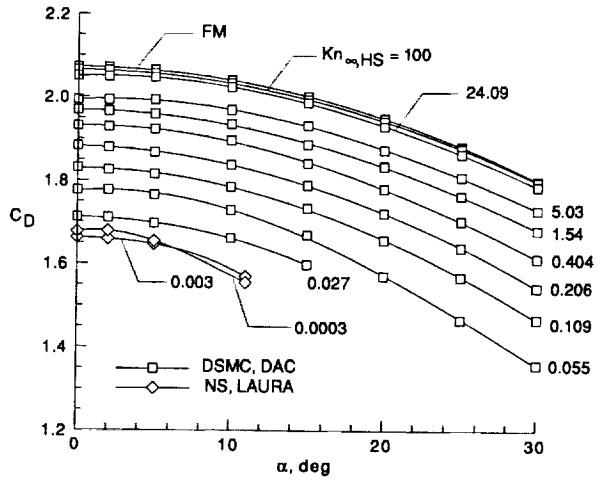

(e) Drag coefficient.
Fig. 5 Continued.

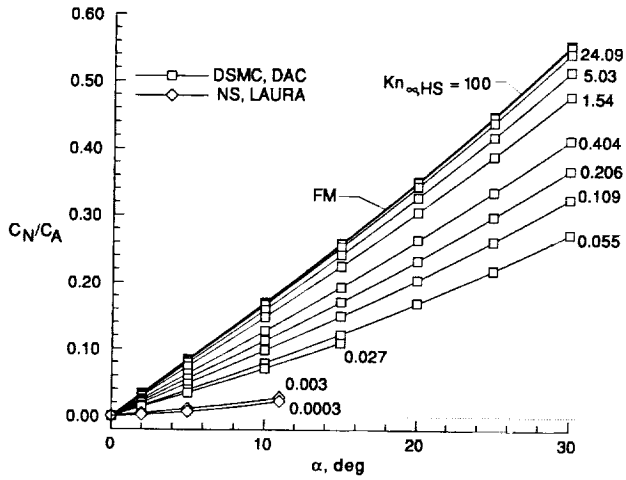

(c) Normal-to axial ratio.
Fig. 5 Continued.

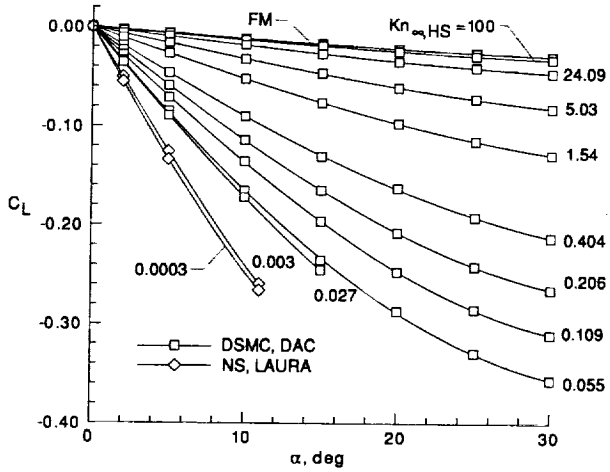

(f) Lift coefficient.
Fig. 5 Continued.

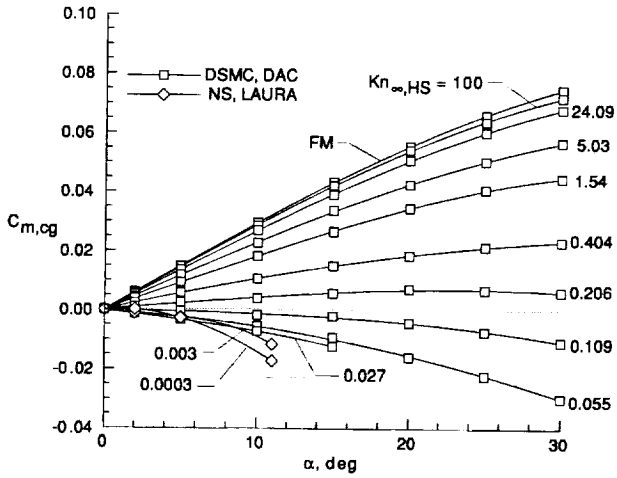

(d) Moment coefficient about center of gravity (x_{cg} = 0.7154 m).
Fig. 5 Continued.

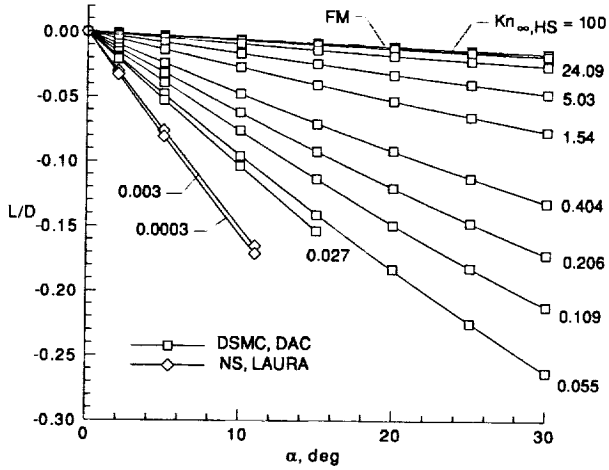

(g) Lift-to-drag ratio.
Fig. 5 Continued.

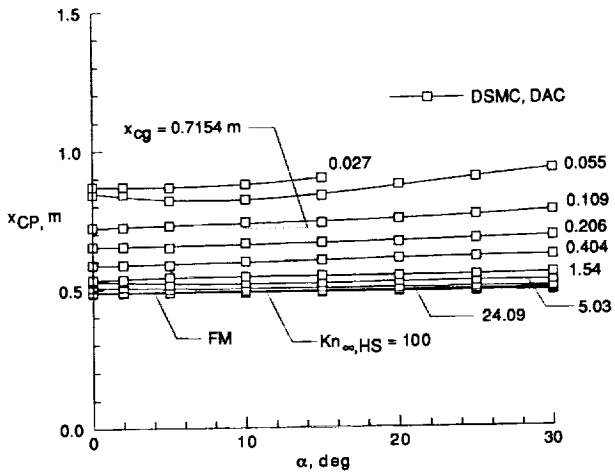

(h) Center of pressure location w.r.t. nose

Fig. 5 Concluded.

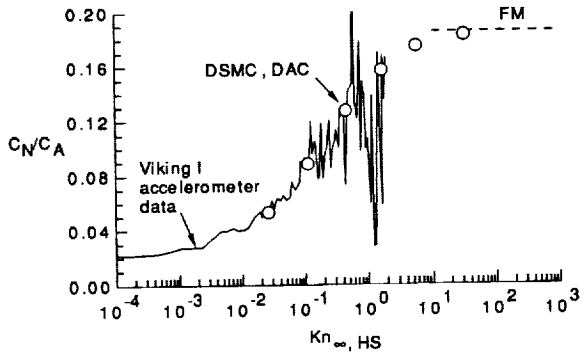

Fig.6 Normal-to-axial coefficient derived from Viking I acceleration measurements compared with DSMC calculations (from Ref. 5).

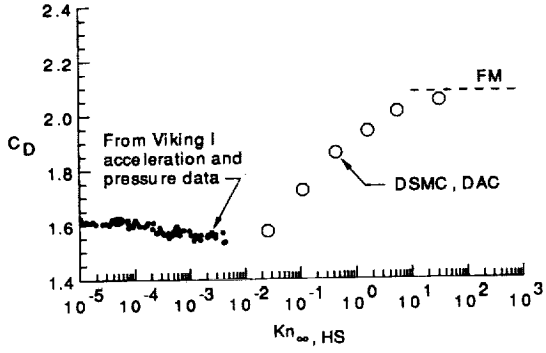

Fig.7 Viking I drag coefficient versus Knudsen number from flight measurements and DSMC calculations (from Ref. 5).

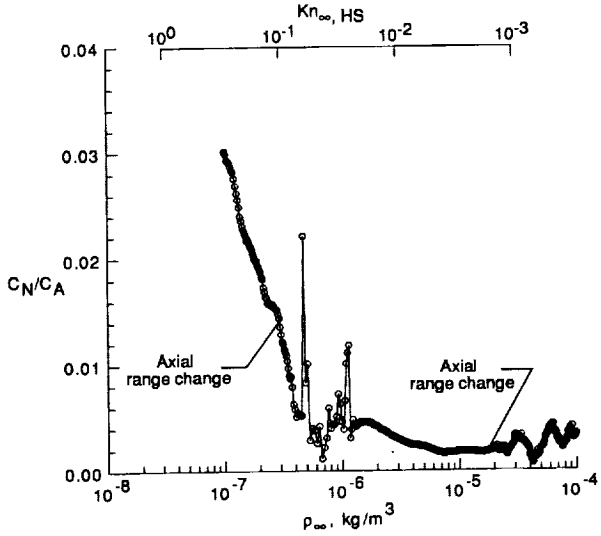

Fig.8 Normal-to-axial coefficient derived from Pathfinder acceleration measurements.

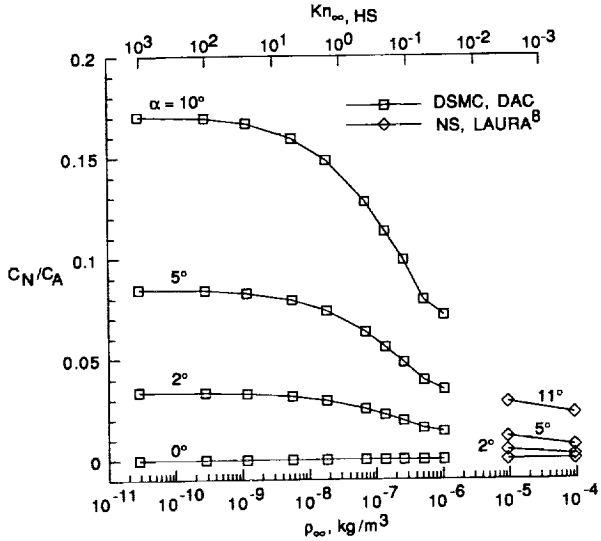

Fig.9 Computed Pathfinder normal-to-axial coefficient.

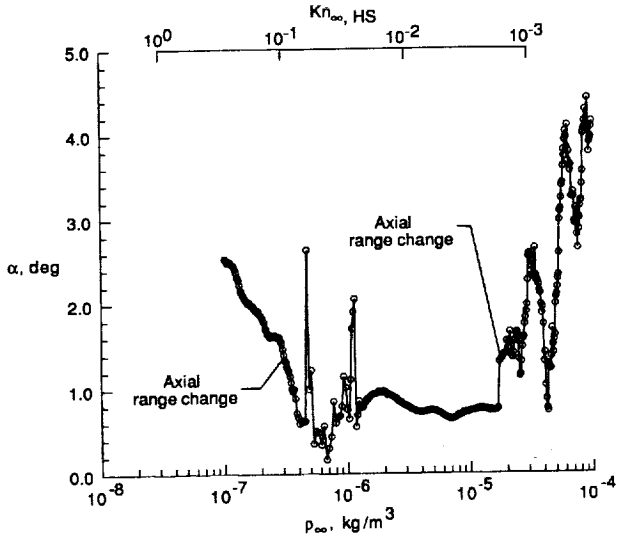

Fig.10 Pathfinder angle of incidence derived from acceleration measurements and computed aerodynamics.

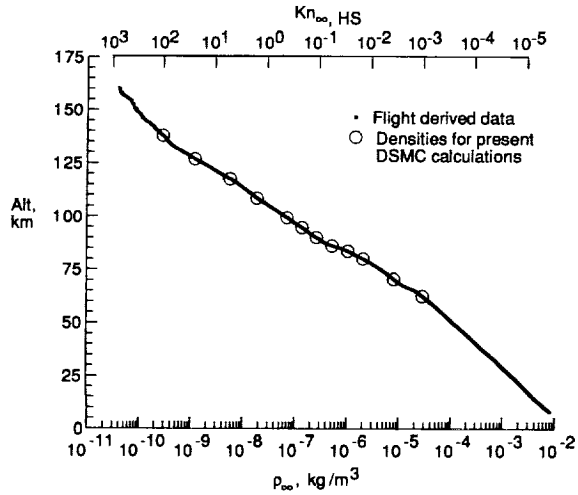

Fig.11 Derived atmospheric density versus altitude from Pathfinder measurements.

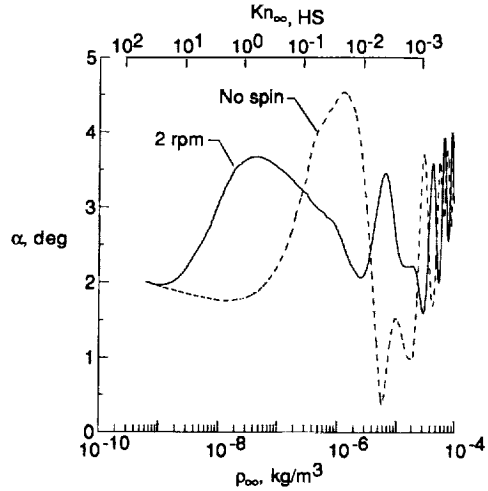

Fig.14 Effect of spin on Pathfinder's attitude from six-DOF simulations.

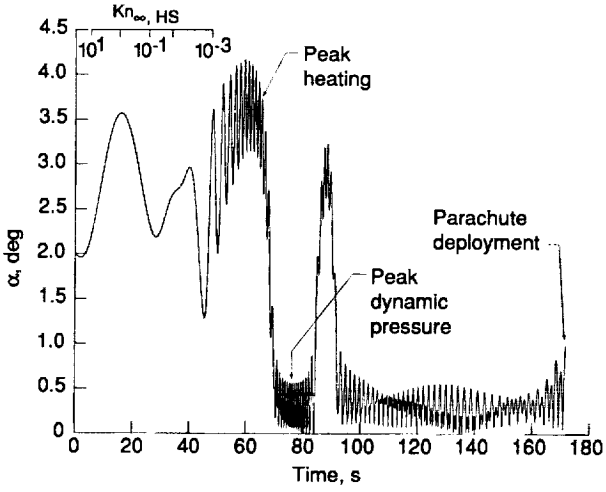

Fig.12 Mars Pathfinder entry attitude profile from an altitude of 132 km using a six-degree-of-freedom simulation.

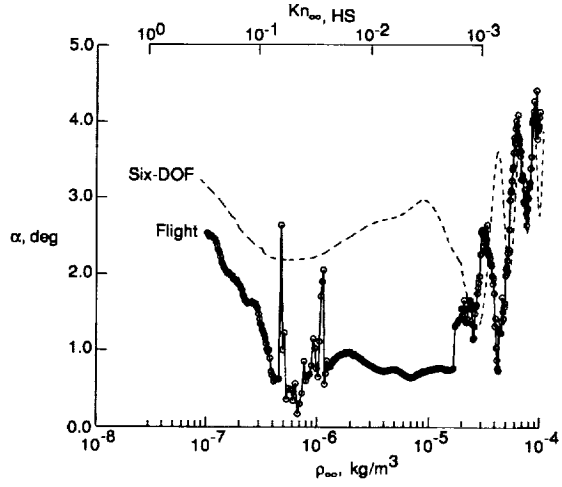

Fig.13 Comparison of flight inferred and six-DOF simulation results for total angle of incidence in the transitional flow regime (time ≈ 21 to 48 s).